Effects of long-term voluntary wheel running and selective breeding for wheel running on femoral nutrient canals

Brandon B. Tan[1], Nicole E. Schwartz[1], Lynn E. Copes[2], Theodore Garland, Jr.[1]

[1] Department of Evolution, Ecology, and Organismal Biology, University of California, Riverside, California, USA

[2] Department of Medical Sciences, Frank H. Netter MD School of Medicine, Quinnipiac University, Hamden, Connecticut, USA

Correspondence
Theodore Garland, Jr., Department of Evolution, Ecology, and Organismal Biology, University of California, Riverside, Riverside, CA 92521, USA.
Email: tgarland@ucr.edu
ORCID ID: 0000-0002-7916-3552

Funding information
Funding was provided by U.S. NSF grants DDIG 0925793 to Lynn E. Copes, as well as IOS-1121273 and IOS-2038528 to Theodore Garland, Jr.

ABSTRACT

The nutrient artery provides ~50-70% of the total blood volume to long bones in mammals. Studying the functional characteristics of this artery in vivo can is difficult and expensive, so most researchers have measured the nutrient foramen, an opening on the outer surface of the bone that served as the entry point for the nutrient artery during development and bone ossification. Others have measured the nutrient canal (i.e., the passage which the nutrient artery once occupied), given that the external dimensions of the foramen do not necessarily remain uniform from the periosteal surface to the medullary cavity. The nutrient canal, as an indicator of blood flow to long bones, has been proposed to provide a link to studying organismal activity (e.g., locomotor behavior) from skeletal morphology. However, although external loading from movement and activity causes skeletal remodeling, it is unclear whether it affects the size or configuration of nutrient canals. To investigate whether nutrient canals can exhibit phenotypic plasticity in response to physical activity, we studied a mouse model in which 4 replicate High Runner (HR) lines have been selectively bred for high voluntary wheel-running behavior. The selection criterion is the average number of wheel revolutions on days 5 & 6 of a 6-day period of wheel access as young adults (~6-8 weeks old). An additional 4 lines are bred without selection to serve as controls (C). For this study, 100 female mice (half HR, half C) from generation 57 were split into an active group housed with wheels and a sedentary group housed without wheels for 12 weeks starting at ~24 days of age. Femurs were collected, soft tissues were removed, and femora were μ-CT scanned at a resolution of 12 microns. We then imported these scans into AMIRA and created 3D models of femoral nutrient canals. We tested for evolved differences in

various nutrient canal traits between HR and C mice, plastic changes resulting from chronic exercise, and the selection history-by-exercise interaction. We found few differences between the nutrient canals of HR vs C mice, or between the active and sedentary groups. We did find an interaction between selection history and voluntary exercise for the total number of nutrient canals per femur, in which wheel access increased the number of canals in C mice but decreased it in HR mice. Our results do not match those from an earlier study, conducted at generation 11, which was prior to the HR lines reaching selection limits for wheel running. The previous study found that mice from the HR lines had significantly larger total canal cross-sectional areas compared to those from C lines. However, this discrepancy is consistent with studies of other skeletal traits, which have found differences between HR and C mice to be somewhat inconsistent across generations, including the loss of some apparent adaptations with continued selective breeding after reaching a selection limit for wheel-running behavior.

Key words: artificial selection; behavior; evolutionary morphology; exercise; femur; *Mus domesticus*; nutrient canal; voluntary wheel running.

1 | Introduction

Bones are dynamic, constantly remodeling in response to changing mechanical needs during growth, load bearing, and locomotion (Frost 1987). Mechanical loading plays an important role in building and maintaining both skeletal mass and strength (Rubin and Lanyon 1984; Newhall et al. 1991; Frost 1997; Huiskes et al. 2000; Mori et al. 2003). When bones experience loading from mechanical forces, the resulting strain induces microdamage to the bone tissue (Seref-Ferlengez et al. 2015). Osteocytes (mechanosensory cells that sense fluid flow associated with strain) then translate mechanical strain to biochemical signals and initiate bone remodeling (Bonewald 2007; Yu et al. 2018). Over the course of bone remodeling, osteoblasts and osteoclasts add or remove bone, respectively (Katsimbri 2017). Thus, exercise that increases the mechanical loading (and strain) on bones can induce changes to traits related to biomechanical properties, such as bone mineral density, mass, and tensile strength (Jones et al. 1977; Gómez-Cabello et al. 2012; Yuan et al. 2016; Karlsson and Rosengren 2020).

Coincident with increased bone remodeling, mechanical loading from exercise also results in increased levels of regional bone and marrow blood flow (Jones et al. 1977; Stabley et al. 2014). Although nutrient, epiphyseal-metaphyseal, and periosteal arteries all supply blood to long bones (Rhinelander 1972), the nutrient artery is often the main source of blood (Trueta 1963; Gümüsburun et al. 1994). The Hagen-Poiseuille equation describes how factors can influence the flow rate through a pipe (e.g., an artery):

$$Q = \frac{\Delta p \pi R^4}{8 \mu L}$$

where flow (Q) is increased when the difference in pressure (Δp) is positive, the radius of the vessel (R) is increased, the viscosity of the medium (μ) is decreased or the length of the vessel (L) is decreased. In particular, changes to the radius of the vessel can have a large effect on flow due to their exponential relationship. Therefore, increased blood perfusion (e.g., due to exercise) can be reasonably attributed to at least some increases in arterial vessel size. Conversely, a study which unloaded the hindlimbs of adult rats by suspending them for two weeks found a significant decrease in nutrient artery maximal diameter compared to controls (Prisby et al. 2015). No studies have yet directly investigated the effect of exercise on nutrient artery diameter. However, measuring the nutrient artery in vivo is difficult, impractical, or in the case of deceased organisms, impossible. Instead, researchers have measured the nutrient foramen (an opening on the outer surface of the bone that is formed when the nutrient artery enters cartilage during endochondral ossification) or the nutrient canal (i.e., the passage which the nutrient artery once occupied) as a proxy for nutrient artery size and, by extension, blood flow to long bones.

Nutrient canals are located in the diaphysis of long bones, and are the entry point for arteries, veins, and peripheral nerves to the medullary cavity (Houssaye and Prévoteau 2020). Given that bone is a hard tissue, one might expect that nutrient canal size limits the maximum size of any vessels that pass through it and so would be positively related to maximal blood flood (e.g., as required during intense periods of bone growth or remodeling). A study of chickens found that nutrient canal area was significantly positively correlated ($r = 0.51$, $p = 0.02$) with the area of the nutrient artery lumen in the femur, although the nutrient artery lumen occupied only ~20% of the nutrient

canal cross section (Hu et al. 2022). This indicates that femoral blood flow rate can, to some extent, be estimated from nutrient canal size. Additionally, nutrient canal size (adjusted for body size) was correlated with the whole-body maximum rate of oxygen consumption during exercise in comparisons among species of mammals, but was less correlated with resting metabolic rate (Seymour et al. 2012). As a result, some have proposed that nutrient canal size can be used as a proxy for the metabolic intensity of extinct animals, such as dinosaurs (Seymour et al. 2012). In kangaroos, during in-pouch development, high growth rate appears to be the main factor determining femoral bone blood flow, while in the post-pouch life stage, micro-fracture repair is most influential on blood flow requirements (Hu et al. 2018). However, despite the intuitive importance of blood flow in the early phases of bone growth and ossification, or whenever bone is remodeling(Sim and Kelly 1970; Gross et al. 1981), relatively little research has been conducted on nutrient canals overall, and, in particular, on whether nutrient canals exhibit phenotypic plasticity in response to behaviors expected to increase blood flow to long bones (e.g., exercise).

The High Runner (HR) mouse model can be used to simultaneously study potential genetic and training effects on bone. Briefly, four replicate lines of mice have been bred for voluntary wheel-running behavior based on the total number of revolutions run on days 5 and 6 of a 6-day exposure to wheels. Four non-selected Control (C) lines are bred without regard to wheel running. HR mice run approximately three times more than C mice on a daily basis, mainly from increased average speed rather than duration (Swallow et al. 1998a; Garland, Jr. et al. 2011; Hiramatsu et al. 2017; Kelly et al. 2017; Copes et al. 2018). HR lines reached an apparent selection limit for wheel running after

~17-27 generations, depending on the replicate line and sex (Careau et al. 2013), and have since continued to run ~2.5-3-fold more than C lines (currently at 102 generations of selection) (Garland, Jr. et al. 2011; Hiramatsu et al. 2017; Kelly et al. 2017; Copes et al. 2018).

HR mice have higher running endurance (Meek et al. 2009) and maximum aerobic capacity (VO_2max) during forced treadmill exercise (e.g., Swallow et al. 1998b; Hiramatsu et al. 2017; Singleton and Garland, Jr. 2019; Cadney et al. 2021; Schwartz et al. 2023), among a number of other anatomical, physiological, neurobiological, behavioral, and genetic differences from C mice (e.g., see Rhodes et al. 2005; Wallace and Garland, Jr. 2016; Singleton and Garland, Jr. 2019; Cadney et al. 2021; Hillis and Garland, Jr. 2023). The HR and C lines have also been shown to differ in skeletal morphology (Kelly et al. 2006; Young et al. 2009; Middleton et al. 2010; Wallace et al. 2012; Schutz et al. 2014; Castro et al. 2022). For example, adjusting for variation in body mass, and depending on the generation studied (See Castro et al. 2021), HR mice have been reported to have increased diameter and mass of hindlimb bones (Kelly et al. 2006), wider distal femora (Middleton et al. 2008), significantly larger periosteal areas, endocortical areas, and polar moments of area in the femur (Wallace et al. 2012), significantly larger femoral condyles (Garland, Jr. and Freeman 2005), and to lack significant hindlimb directional asymmetry, which is present in control mice (Garland, Jr. and Freeman 2005). However, hindlimb length and metatarsal-to-femur ratio, which are classic indicators of cursoriality, were not increased in HR mice (Garland, Jr. and Freeman 2005; Castro et al. 2022). A previous study of the nutrient canals of both HR and C mice was conducted at generation 11, prior to the selection limit, finding that HR

mice had significantly higher nutrient canal total cross sectional area in both sexes (Schwartz et al. 2018).

The purpose of the present study was to investigate (1) whether previously studied differences in nutrient canal size between HR and C lines (Schwartz et al. 2018) were still present at a later generation (i.e., after selection limits had been attained), and (2) whether nutrient canal cross-sectional area exhibits phenotypic plasticity in response to chronic exercise. We studied the same 100 females from generation 57 that have been previously examined in Copes et al. (2015, 2018), Lewton et al. (2019), and Castro et al. (2022). Given that the HR mice used for the present study ran much more than C mice from weaning (3 weeks) to 15 weeks of age (Copes et al. 2018), we expected that any effects of chronic exercise, if present, would be greater in HR than in C mice.

2 | Methods

2.1 | Selection experiment background and experimental design

As noted above, the specimens used here are the same as in Copes et al. (2018), and were sampled from generation 57 of the High Runner (HR) selection experiment (Swallow et al. 1998a), as outlined in the Introduction. (The selection experiment has since passed 100 generations.) Briefly, we sampled a total of 100 females, equally divided between the four replicate HR and four non-selected Control (C) lines, except that HR line 6 included four extra mice because it is polymorphic for the mini-muscle phenotype (see below). Mice were weaned and weighed at 21 days of age.

The 12 weeks of experimental procedures began when the mice were 24-27 days old, and then housed individually, half in cages with an attached wheel (see below) and half without. Mice reach sexual maturity at ~6 weeks of age (Jilka 2013) and experiments involving bone changes in mice typically last 8 to 12 weeks, because bone

191 growth slows substantially after puberty (Bourguignon 1988; Jilka 2013). Weekly
192 procedures included weighing of each mouse and food hopper, from which apparent food
193 consumption was determined (Swallow et al. 2001), as reported elsewhere (Copes et al.
194 2015, 2018). All experimental procedures were approved by the Institutional Animal Care
195 and Use Committees at the University of California, Riverside and Arizona State
196 University.

197 ## 2.2 | Wheel running

198 At ~24 days of age, half of the mice were given wheel access, as used in the
199 selection protocol (1.12 m circumference) (Swallow et al. 1998a). Each of the four
200 groups (Control No Wheel, Control Wheel, HR No Wheel, HR Wheel) began with 25
201 mice. The term "active" will be used to refer to the groups with access to wheels whereas
202 those without access to wheels are referred to as "sedentary." Each day, a computer
203 recorded wheel revolutions in 1-minute intervals over a period of 23.5 hrs. We calculated
204 the total number of revolutions, the number of 1-min intervals with at least one revolution
205 (minutes of wheel activity), the mean speed of running (revolutions/intervals), and the
206 single interval with the greatest number of revolutions (maximum speed) using SPSS
207 (IBM). We used average values for wheel running across 12 weeks, which have been
208 reported previously (Copes et al. 2018), as covariates to predict bone traits.

209 ## 2.3 | Spontaneous physical activity in the home cage

210 All 100 cages were fitted with a passive infrared sensor placed in a corner and
211 housed in a wire mesh protective enclosure (Copes et al. 2015). Total home-cage
212 activity (HCA) was taken as the sum of all activity over 23.5 hours, HCA duration was
213 calculated as the number of 1-min intervals during which any activity was registered, and
214 mean intensity of activity was calculated as total HCA divided by minutes of activity.

Similarly to wheel running, we used the average values of HCA over 12 weeks, reported in Copes et al. (2018), as covariates in statistical analyses.

2.4 | Dissections and specimen preparation

Over the course of the experiment, three mice died of various causes. The remaining 97 were euthanized by CO_2 overdose. The triceps surae muscles were weighed and their mass was used to determine the number of mice with the mini-muscle phenotype (Kelly et al. 2013); 18 mice were found with the trait in this sample. Any tissue not taken at dissection and discarded or removed via soaking of the carcass in a 1% solution of enzymatic detergent (marketed as Tergazyme by Alconox). Starting with N = 100 mice, 3 mice died prior to collecting femurs, and 3 of the CT scans (see below) had too much static, making them unusable for measuring nutrient canals, for a final N of 94 for measuring nutrient canals.

2.5 | µCT scanning

The right femur of each specimen was µCT scanned at the University of Calgary (Viva-CT40, Scanco Medical AG, Basserdorf, Switzerland) at 12-µm resolution (55 kV, 145 mA, 500 projections) (Copes et al. (2018) erroneously listed the resolution as 21 µm.) The femur was chosen because, along with the humerus, they are the largest long bones with the greatest attached muscle mass, (2) are the most frequently examined in studies of the effects of exercise on bone morphology (Ferguson et al. 2003; Judex et al. 2004; Yang et al. 2007; Tommasini et al. 2008; Jepsen et al. 2009), and (3) were previously used to study nutrient canal morphology in HR mice (Schwartz et al. 2018).

2.6 | AMIRA 3D modeling

For each specimen, the raw data were reconstructed as 16-bit TIFF image sequential stacks using ImageJ software (Schneider et al. 2012). Image stacks were

239 imported into Thermo Scientific AMIRA 5.6 Software, Thermo Fisher Scientific (Waltham,
240 Massachusetts, USA) for visualization and segmentation.

241 We followed the protocols previously established in Schwartz et al. (2018) for 3D
242 modeling of femurs from CT scans and nutrient canals. The Supplementary Material
243 contains a PDF file with detailed instructions. Using the *Isosurface* module in AMIRA,
244 surface renderings of the femur were created, and the external morphology of the nutrient
245 foramina (defined here as the superficial openings through which the nutrient artery(s) is
246 presumed to pass) were inspected. Examination for nutrient foramina was restricted to a
247 portion of the bone inferior to the femoral neck and superior to the proximal edge of the
248 patellar groove (Figure 1). This restriction was used in order to exclude metaphyseal and
249 epiphyseal blood vessels, which typically penetrate bone outside of this region, although
250 at least in mice the bottom third of the femur can also contain metaphyseal vessels
251 (Brookes 1958; Bab et al. 2007; Prisby 2020). Our criteria for identification of a nutrient
252 canal required a continuous absence of cortical bone from the periosteal (external)
253 border of the cortex, through the cortex, and past the endosteal surface towards the
254 medullary cavity. After identification, the empty space of the nutrient canal was manually
255 selected slide-by-slide in AMIRA (Figure 2). Using the *Label Field* module, a 3D surface
256 model of the nutrient canal was created. Once all the nutrient canals in the bone had
257 been selected and modeled, each canal was isolated from the femur and virtually re-
258 oriented using the *Align Principal Axes* function. The nutrient canals were re-oriented so
259 that a transverse cross-section could be obtained perpendicular to the long axis of the
260 canal (Figure 3). This was necessary to avoid elliptical cross-sections, which would
261 overestimate the area compared to the correct circular cross section. Ten cross-sections

of the nutrient canal were measured for area, and the minimum cross-sectional area of the total nutrient canal was recorded. The minimum cross-sectional area was chosen because the flow through a cylindrical pipe is limited by the smallest cross-sectional area as described by the Hagen-Poiseuille equation: $Q = (P\pi r^4)/(8L\eta)$, where Q is flow rate, P is the difference in blood pressure, *L* is vessel segment length, η is blood viscosity, and r is the radius of the vessel.

Because of the varied size and shape of nutrient canals, including both non-linear or curved shapes and bifurcations, certain canals required multiple rounds of re-orientation as described above. For nutrient canals with a curved shape, the long axis was re-oriented several times along the length of the canal at each major inflection point (assessed visually) so that multiple perpendicular cross-sections could be obtained. Only the smallest cross-sectional area was used for further analysis.

In nutrient canals with bifurcation, all the branches of the canal were measured for minimum cross-sectional area as described above. If the sum of the minimum cross-sectional area of the branches was greater than that of the source trunk, then the branches were not considered blood-flow limiting structures and the minimum cross-sectional area of the trunk was recorded (see slide 37 in Nutrient_Canal_Methods_Presentation_6.pdf of the Supplemental Material). If the cross-sectional area of the source trunk was greater than the sum of its branches, then the branches were considered as blood-flow limiting. In this case, both branches were counted as distinct nutrient canals, each with their own minimum cross-sectional area.

Although not measured in Schwartz et al. (2018), the location of each nutrient canal was also recorded by noting the slide on which the nutrient canal started and

ended. Those numbers were averaged to obtain the midpoint of the nutrient canal. The start and end slide of the whole femur was also recorded. The nutrient canal's position along the bone as a proportion of its length was calculated.

As compared with Schwartz et al. (2018), another change to the methodology included the adjustment of the *Zoom and Data Window* as well as the *Display and Masking* parameters. Previously, these parameters were both adjusted on a case-by-case basis. This parameter is of particular importance because it determines what AMIRA considers to be bone versus empty space, which will directly affect the size of the minimum cross-sectional area of all nutrient canals measured for that bone. Compared to the previous study, the CT scans from the current study had much more static noise, which made measurements more sensitive to variation in masking values. To lower possible sources of error, we elected to use standardized *Zoom and Data Window* as well as *Display and Masking* values across the entire data set. These values were obtained by having 2 researchers each produce 2 replicates of the aforementioned values for a total of 4 values for every parameter of every bone. The values were then compared, discrepant values were re-examined, and all values were then averaged across the entire data set.

Additionally, having the correct number of nutrient canals is important for measuring the total cross-sectional area correctly, as well as for analyzing the number of nutrient canals themselves. We confirmed each nutrient canal between 2 researchers for each of the 94 bones, checking that the nutrient canals were within the previously established borders, as well as fully penetrating the periosteal border, past the endosteal

surface to the medullary cavity. This step was included because many nutrient canals were found much closer to the borders previously established in Schwartz et al. (2018).

2.7 | Statistical analyses

Following numerous previous studies of these lines of mice (e.g., Copes et al. 2015, 2018; Lewton et al. 2019; Castro et al. 2022), data were analyzed as mixed models in SAS Procedure Mixed, with REML estimation and Type III Tests of Fixed Effects. Main effects were linetype (selected HR lines vs. non-selected C lines), activity (active vs. sedentary), and the mini-muscle phenotype (see below). Replicate line was nested within linetype as a random effect. Degrees of freedom for linetype, activity, and the linetype-by-activity interaction were 1 and 6. Analyses were done with and without body mass as a covariate. Additional analyses were done with wheel running and/or home-cage activity (averaged across the entire 12-week exposure to wheels) as covariates (Copes et al. 2018). Statistical significance was evaluated at $P < 0.05$. Outliers were removed if the absolute value of their standardized residual exceeded ~3 and/or the value was >1 standard deviation from the next value. For analysis of canal branching, scored as 0 for none or 1 if one or more branching canals occurred in a given femur, we used similar mixed models, but with SAS Procedure GLIMMIX.

The mini-muscle phenotype (Garland, Jr. et al. 2002) is caused by a Mendelian recessive mutation (Kelly et al. 2013) that halves hindlimb muscle mass, primarily due to a great reduction in the number of Type IIb muscle fibers (Talmadge et al. 2014), with many pleiotropic effects, such as generally larger internal organs (Garland, Jr. et al. 2002; Swallow and Garland, Jr. 2005; Kelly et al. 2017). Various skeletal traits are altered in mini-muscle individuals, including lengthening and narrowing of the femur (e.g., Kelly et al. 2006), lower femoral cortical areas and bending moments of inertia (Copes et

al. 2018), as well as smaller femoral third trochanters (Castro et al. 2022). Mini-muscle mice also have smaller ilium cross sectional properties, including cortical area, total periosteal area, polar section modulus, polar moment of area, and cortical area robusticity index (Lewton et al. 2019). The underlying allele was initially present at a frequency of ~7% in the base population. The mini-muscle phenotype was observed in two of the four HR lines, eventually becoming fixed in one HR line (HR line 3) and remaining polymorphic in another (HR line 6). The mini-muscle phenotype was observed in one C line for at least 22 generations, then lost. Of the 94 mice analyzed here for femoral canal properties, 11 in HR line 3 and 5 in HR line 6 were mini-muscle.

3 | Results

3.1 | Body mass, body length, femur length

No statistically significant main effects or interactions were found for body mass, body mass with body length as a covariate, body length, or femur length with body mass or body length as a covariate (Table 1). Results were similar when the physical activity covariates were included (Supplemental Table S1). The sample size for these traits differs by a few mice because three of the CT scans had scanning errors and were unusable for measuring nutrient canals. Additionally, a few of the mice that were used for measuring nutrient canals did not have measurements for femur and/or body length. In any case, the findings for body mass and femur length are consistent with those reported in Copes et al. (2018), while analysis of body length was not previously reported.

3.2 | Basic characteristics of nutrient canals

As noted previously (Schwartz et al. 2018), nutrient canals in mouse femora are diverse in shape, as well as size and number. In the present study, canals varied in shape from straight tubes through the bone to complex curved, looped or branched

canals (Figure 3). Canal numbers ranged from 0 to 5 in the proximal region, 0 to 5 in the distal region, and 1 to 7 in total.

Some canals were bifurcated, but the number was relatively small (7 of 167 canals in the 47 HR mice [4.2%], 29 of 188 canals in the 47 C mice [15.4%]). When analyzed as a 0-1 variable indicating whether a given mouse had any bifurcated canals (SAS PROC GLIMMIX) and with line nested within linetype and no covariates, HR mice (5 of 47 had at least one bifurcated canal) tended to have more bifurcated canals ($P = 0.0631$) than did C mice (18 of 47 had at least one bifurcated canal), with no effect of activity, no linetype-by-activity interaction, and no effect of mini muscle (Table 3). No variance was associated with line-within-linetype, and an analysis without line nested and no covariates indicated a linetype effect ($P = 0.0252$), again with no other significant main effects. Models with mass as a covariate indicated no effect of body mass (Table 3).

Some canals were curved: 63 of 167 canals in HR lines (37.7%) and 88 of 188 canals in C lines (46.8%). Canals were classified as either straight or curved, with straight canals having no noticeable curve or bend, and everything else being classified as curved (curved, looped, etc). In analyses from SAS PROC MIXED, we found no statistical effects on the percentage of curved canals.

Location of each nutrient canal was recorded, but for ease of analysis, nutrient canals were designated as proximal or distal based on their respective location, and the average proximal and distal locations were calculated. Average distal canal location had no main effects but was associated with body mass ($P = 0.0379$), with distal canals being located closer to the midpoint of the bone as mass increased. This effect was equally strong in analyses with the activity covariates ($P = 0.0283$) (Supplemental Table S1), and

in those analyses average distal canal location was more medial as wheel running increased (P = 0.0350).

3.3 | Nutrient canal numbers

The total number of nutrient canals per femur was affected by a significant linetype-by-activity interaction (Table 1: P = 0.0175). Specifically, for C mice, wheel access increased canal number, whereas for HR mice, wheel access decreased the total number of canals (Figure 4). This interaction also affected proximal and distal numbers of canals in the same manner, but statistical significance was not attained (P = 0.1378 and 0.0949, respectively). Body mass was a negative predictor of proximal number (P = 0.0188) but a positive predictor of distal number (P = 0.0056), resulting in no significant relation with total canal number (P = 0.6773). Results were similar when body mass was not included as a covariate (Supplemental Table S1).

Percent distal number (distal canals / total canals) had an effect of linetype (P = 0.0493), with C mice having lower percentage of distal canals and HR mice having higher percentage of distal canals. However, this effect was only present in the analysis with mass, wheel running, and home cage activity as covariates. Percent distal number decreased with home cage activity (P = 0.0330). Without mass as a covariate, this effect lost its statistical significance (P = 0.0822).

3.4 | Nutrient canal cross sectional areas

Total nutrient canal area, as well as proximal and distal canal area, were unaffected by linetype, activity, linetype-by-activity interaction, or mini muscle. However, body mass was a significant positive predictor (P = 0.0032) of distal canal area, but not total or proximal area (P = 0.2026 and 0.2186, respectively) (Table 2). Additionally,

401 percent distal cross-sectional area (distal area / total area) also increased with mass (P =
402 0.0342). These effects were equally strong when activity covariates were included.

403 ## 4 | Discussion

404 We studied the number, location, size, and shape of femoral nutrient canals from
405 four replicate High Runner (HR) lines of house mice that had been selectively bred for
406 voluntary wheel-running behavior for 57 generations, and compared with four non-
407 selected Control (C) lines. Half of the mice were housed with wheels (active group) and
408 half without (sedentary group) for 12 weeks starting shortly after at weaning. With this
409 experimental design, we were able to study evolved differences related to selection for
410 high voluntary wheel-running behavior (HR vs. C lines), phenotypic plasticity in response
411 to chronic exercise across a key stage of ontogeny (active vs sedentary), and potential
412 interactions between the two factors.

413 A previous study examined femoral nutrient canal morphology at generation 11
414 and found that HR lines had a significantly greater total canal area than C lines.
415 However, the HR lines from that study had not yet reached a selection limit (plateau) for
416 voluntary wheel-running behavior (which would not occur until ~10 generations later
417 (Careau et al. 2013)). Therefore, we expected that the HR vs C difference might have
418 increased by our sampling at generation 57. In addition, presuming that the size (but not
419 number) of canals can change between weaning and the attainment of full skeletal
420 growth, we expected that voluntary exercise (especially in the HR lines) would lead to
421 changes in nutrient canal size. Contrary to our expectations, we found little evidence of
422 differences between the HR and C lines at generation 57, nor of an exercise-training

423 effect, although we did find a significant linetype-by-activity interaction for the total
424 number of canals in the femur (see Section 4.2).

425 ## 4.1 | Summary of nutrient canal characteristics

426 Historically, nutrient canals have been described as a single foramen, with no
427 branching, oriented at a right angle to the long axis of long bones, which develop an
428 oblique orientation over time due to asymmetric bone growth (Greene 1935; Rogers and
429 Gladstone 1950; Brookes and Harrison 1957; Brookes 1958; Henderson 1978; Singh et
430 al. 1991). In general, previous studies of larger-bodied animals (e.g., humans, pigs,
431 horses) have described most long bones as possessing only one nutrient foramen,
432 though some may have two or none at all (Payton 1934; Carroll 1963; Campos et al.
433 1987). However, more recent studies using micro-CT scans and 3D modelling software
434 have shown great amounts of variation in both the number and structure of nutrient
435 canals, including the presence of branching in some nutrient canals (Hu et al. 2018;
436 Schwartz et al. 2018; Houssaye and Prévoteau 2020). In the femur, nutrient canals are
437 most often oriented proximo-distally, from the inside to the outside of the bone (Houssaye
438 and Prévoteau 2020). Studies with multiple species have shown a great amount of both
439 inter- and intra-specific variation in the number of nutrient canals per long bone
440 (Houssaye and Prévoteau 2020). Our previous study of 137 mice found that femurs
441 averaged between four and five nutrient canals, and that nutrient canals were located
442 near the proximal or distal ends, with no nutrient canals being found in the middle of the
443 diaphysis (Schwartz et al. 2018). The current study found nutrient canal locations to be
444 the same as previously noted.

445 As expected from our previous study (Schwartz et al. 2018), we encountered a
446 large diversity of nutrient canal shapes, ranging from straight tubes, to curved, looped or

bifurcating canals (see also Houssaye and Prévoteau 2020). Only three of 94 mice had exclusively straight canals (i.e., nutrient canals that neither curved nor branched); 88 had at least one “curved” canal (which we defined as any canal needing more than one round of re-orientation during the measurement process, as described in section 2.6), and 38 mice had more than one “curved” canals. With regard to bifurcation, 71 mice had no branched canals, 21 had one, and only two had two. Although the functional significance of canal bifurcation is unknown, we found that HR mice tended to have a greater number of bifurcated canals compared to C mice (Table 3, SAS PROC GLIMMIX, P = 0.0631). Something interesting about the aforementioned bifurcation of nutrient canals is that these bifurcations occur *within* the cortical bone. Although noted in Schwartz et al., (2018), we add here that this phenomenon is odd in that bifurcation before or after entering the cortical bone would be, at least in principle, a simpler and more efficient process. Whether this has any functional implications is currently unknown.

4.2 | Nutrient canal numbers

Total nutrient canal number was affected by a significant linetype-by-activity interaction (Table 1: P = 0.0175 without correction for multiple comparisons), with wheel access increasing canal number for C mice (+15%) but decreasing it for HR mice (-6%). This result is perhaps surprising, especially given that no such effects, nor indeed any effects of exercise, were found for femur length, cortical cross-sectional area, or polar moment of inertia (Copes et al. 2018). Similarly, no effects of exercise nor any interactions were found for the sizes of three femoral muscle attachment sites (Castro et al. 2022).

Nutrient canals are first formed during development, when the nutrient artery penetrates the cartilaginous femur prior to endochondral ossification (Ahn 2013). In

mice, ossification of the femur starts at around 14.5 days post coitum (Barle and Piano 2008). No mechanism for new nutrient canals to form after ossification is presently known. Formation of new blood vessels within bone is possible, referred to as intraosseous angiogenesis (Laroche 2002; Rumney et al. 2019; Rodrigues et al. 2022). However, this process refers to the growth of new capillaries from preexisting capillaries or from postcapillary venules, and whether or not this process can occur within nutrient canals is unknown (Laroche 2002). Despite this, we can speculate as to how chronic exercise on wheels might affect the number of nutrient canals. Perhaps mice at weaning have more canals than needed, with some closing as they grow and age to sexual maturity and beyond. If all mice have an excess number of nutrient canals at weaning (consistent with the idea of "momentarily excessive construction" in Gans 1979), then perhaps those from the relatively low-activity C lines need to keep more canals to accommodate chronic voluntary wheel running, whereas HR mice, which run much more, need to divert more blood flow to the trabecular bone at the ends of the femur, which occurs via canal closing.

Closing of a canal would decrease blood flow to the center of the femur and thus divert flow to the trabecular bone at the ends of the femur via metaphyseal and epiphyseal blood vessels. Ten weeks of treadmill running in young growing rats resulted in increased trabecular bone mass, from creation of new trabeculae, as well as increased trabecular thickness (Joo et al. 2003). A closing mechanism might involve arteries and/or veins that run through the canals withering, followed by the empty canal being filled in by ossification.

The mechanism of arteries/veins closing could be similar to a process known as

vascular rarefaction, which occurs in arterioles and capillaries (Rosei and Rizzoni 2007). Vascular rarefaction occurs in hypertensive animals (Goligorsky 2010; Liang et al. 2019). However, the HR mice have not been found to be hypertensive (Kolb et al. 2013), so although the mechanism of nutrient canals closing may not be exactly as follows, we believe it is important to acknowledge the possibility. Rarefaction can occur in two ways, functional and structural rarefaction, where functional rarefaction is a reversible reduction in perfusion and structural rarefaction is an anatomical loss of vessels (Chen et al. 1981). Structural rarefaction is likely preceded by functional rarefaction (Prewitt et al. 1989). However, we know of no evidence that closing of canals occurs in mice after weaning, regardless of the mechanism. This could be an area for future study.

A recent comparative study analyzed nutrient canals in the femur and humerus from 23 different quadrupedal mammal species, including 10 mustelids (Houssaye and Prévoteau 2020). The study group was phylogenetically diverse, as well as diverse in size, morphology, and method of locomotion, as it included terrestrial, semi-aquatic, and aquatic organisms (Houssaye and Prévoteau 2020). Some of the species were represented by more than one femur sample, giving a total sample size of 48 femurs. The number of nutrient canals found in a single femur ranged from 1-4, with an average number of 2 canals per femur (mean = 1.96). The species from this study were all larger than the mice in the present study, which had between 1 and 7 nutrient canals (mean = 3.78). Taking averages from each species from their data, ours, a value for rats of one canal (Brookes 1958; Henderson 1978; Prisby et al. 2015; Prisby 2020), and an average of two for humans (Gupta and Ambekar 2016), the correlation between the average number of femoral nutrient canals and average body length (determined from Wikipedia)

was -0.11, which is not statistically significant (N = 25 species but 26 data points (mice represented twice), P = 0.59). Although not discussed in Houssaye and Prévoteau (2020), allometry does not seem to be a factor in explaining interspecific variation in nutrient canal number.

Another possibility to consider would be the presence of metaphyseal canals in the diaphysis, where nutrient canals were being measured. Metaphyseal canals exiting the bone in the diaphysis have been observed by Houssaye and Prévoteau (2020) in multiple species of mammals. In further support of this possibility, the metaphyseal zone in murine femurs extends partly into the diaphysis (Bab et al. 2007). Metaphyseal canals in the diaphysis would be a possible imperfection to the data, which could introduce error in the number and total area of nutrient canals. However, potential metaphyseal canals were inspected by two researchers on the basis that only nutrient canals would be (a) complete from the outer surface of the cortical bone to the medullary cavity and (b) oriented towards the midpoint of the diaphysis (i.e., pointed away from the metaphyseal region of bone). Therefore, we believe that the chance of including metaphyseal canals in this data set are minimal.

4.3 | Nutrient canal cross-sectional areas

Our results did not replicate those of a previous study conducted at generation 11, prior to when the HR lines reached selection limits (plateaus), which found HR mice to have significantly higher total cross sectional area of femoral nutrient canals compared to C mice (Schwartz et al. 2018). This discrepancy is perhaps not surprising, given that another study found skeletal differences between HR and C mice to fluctuate across generations (Castro et al. 2021).

4.4 | Concluding remarks and future directions

In the present study of 16 traits related to femoral nutrient canals, we found no statistically significant ($P < 0.05$) effects of linetype, activity or the mini-muscle phenotype, and only a single linetype-by-activity interaction ($P = 0.0175$). This number of significant effects (1/64 = 1.6%) is lower than observed for other bone traits studied in these same individual mice, especially for the mini-muscle effect (Table 2). Tallying across three previous studies that reported 22 bone traits (Copes et al. 2018; Lewton et al. 2019; Castro et al. 2022), the number of traits with $P < 0.05$ was 0/22 for linetype, 3/22 (14%) for activity, 0/22 for the linetype-by-activity interaction, and 8/22 (36%) for the mini-muscle phenotype (grand total 11/88 = 12.5%). With respect to body mass as a covariate, we also found a smaller number of significant effects (44% here versus 86%). Taken together, these results indicate that, at least for these mice and this type of exercise exposure, nutrient canals are both less phenotypically plastic and less likely to respond evolutionarily to selection for increased locomotor activity than many other osteological traits. However, phenotypically plastic characteristics of nutrient canals may be more closely related to factors in embryonic development when bone is first changing from cartilage into ossified bone, a life stage that was not examined in the current study. In addition, characteristics might have changed at the histological level (e.g., bone remodeling), but again we did not examine that here.

A possible explanation for the lack of skeletal change induced by 12 weeks of wheel-running in these mice is that their bones were affected by activity, just not in traits that were measured. For example, forced treadmill exercise for five weeks in young mice increased tibial bone strength and post-yield behavior without significant changes in bone mass or architecture (Gardinier et al. 2018). More specifically, no exercise effects were

found for cortical area or polar moment of inertia, which is consistent with the findings of Copes et al. (2018), who analyzed the femur and humerus. However, Lewton et al. (2019) did find that activity increased the cortical area of the ilium. Bone strength and post-yield behavior have not been studied in this set of mice, and given the way the bones were cleaned and stored, it will be impossible to do so in the future, so any effect of activity on those traits in this specific set of mice is unknown.

Although the nutrient artery is the primary source of blood to long bones, metaphyseal and epiphyseal arteries also supply blood to long bones (Brookes 1958; Trueta 1963; Gümüsburun et al. 1994; Prisby 2020). For example, when the nutrient canal of day-old rabbits was occluded, adult femurs were only 3% shorter compared to controls (Brookes 1957). Thus, the metaphyseal and epiphyseal arteries were able to accommodate and supply most of the blood that would have otherwise been provided by the nutrient artery (Brookes 1957). Additionally, mice have hundreds of capillaries that fully cross the cortical bone from the endosteum to the periosteum (Grüneboom et al. 2019). Perhaps these transcortical vessels were able to supplement the blood flow to long bones in addition to the nutrient artery. The current study used 12-μm resolution CT scans, which are not sufficient to detect capillaries, which are usually 8 to 10 μm in diameter. Some studies suggest that the periosteum, the outer layer of long bones, may be permeable in certain conditions (Li et al. 1987; Qin et al. 2003; Evans et al. 2013). For example, the periosteum was found to increased its permeability with loading when compared to unloaded bone, as well as exhibiting differences in directional permeability, dependent on flow rates (Knothe Tate et al. 1998; Evans et al. 2013). If the periosteum is permeable, then nutrients and waste products could enter and exit through the bone itself

587 instead of having to pass through the nutrient canal. This would reduce or neutralize the
588 need for nutrient canal plasticity to accommodate changing demands in bone growth and
589 remodeling. However, this diffusion mechanism of transport is likely more useful for
590 transporting small molecules, such as amino acids, rather than larger molecules, such as
591 proteins (Knothe Tate et al. 1998). Additionally, the permeability of the periosteum in a
592 mouse model has not yet been studied. Future studies should examine the adaptability
593 of the bone's blood supply, and how this adaptability varies depending on genetic or
594 environmental factors.

595 How nutrient canals can change in size and number throughout development
596 needs further investigation. For future studies, vascular contrast perfusion in conjunction
597 with CT scans (or perhaps contrast-enhanced MRI) could be used to more precisely
598 study nutrient canals in vivo and the various nerves, arteries, and veins that pass through
599 them. Vascular contrast perfusion has been used in chickens to study the size of the
600 nutrient artery in relation to its nutrient canal (Hu et al. 2022), but chickens differ in the
601 number of nutrient canals compared to mice, with a maximum of three per femur and
602 most femurs having only one nutrient canal. 18F-labeled sodium fluoride -([18F]NaF)
603 imaging with positron emission tomography (PET) could be utilized to investigate
604 possible shifting of perfusion and remodeling activity between the diaphysis and
605 metaphyseal region of the femur. In addition, microsphere injection could be used to
606 measure blood supply to the bone. Another area that needs further investigation is the
607 functional significance of nutrient canal number.

608 Although nutrient canal number clearly varies both among and within species
609 (Schwartz et al. 2018; Houssaye and Prévoteau 2020; present study), symmetry between

bones has not yet been examined. Given that the asymmetry of hindlimb bone length was found to be reduced in the HR lines of mice at generation 11, this would be an interesting area for future research.

ACKNOWLEDGEMENTS

We thank Alberto A. Castro for assistance with image analysis.

CONFLICT OF INTEREST

The authors declare no conflict of interest.

AUTHOR CONTRIBUTIONS

All authors designed the research. L.E.C. and T.G. produced the mice. L.E.C. obtained the CT scans. B.B.T. and N.E.S. designed the methodology used to acquire data and acquired the data. B.B.T. and T.G. performed the analyses and drafted the manuscript. All authors revised the manuscript.

DATA AVAILABILITY

Data are available on request from the authors.

ORCID

Theodore Garland Jr. https://orcid.org/0000-0002-7916-3552

Nicole E. Schwartz https://orcid.org/0000-0002-7411-3011

References

Ahn, D. 2013. Anatomical study on the diaphyseal nutrient foramen of the femur and tibia of the German Shepherd dog. J. Vet. Med. Sci. 75:803–808.

Bab, I., C. Hajbi-Yonissi, Y. Gabet, and R. Müller. 2007. Femur and hip joint. Pp. 161–169 *in* I. Bab, C. Hajbi-Yonissi, Y. Gabet, and R. Müller, eds. Micro-tomographic atlas of the mouse skeleton. Springer US, Boston, MA.

Barle, L. E., and Z. J. Piano. 2008. Development of the skeleton in mouse fetuses of both sexes between 14.5 and 18.5 days post coitum. Pol. J. Vet. Sci. 11:147–149.

Bonewald, L. F. 2007. Osteocytes as dynamic multifunctional cells. Ann. N. Y. Acad. Sci. 1116:281–290.

Bourguignon, J.-P. 1988. Linear growth as a function of age at onset of puberty and sex steroid dosage: therapeutic implications. Endocr. Rev. 9:467–488.

Brookes, M. 1957. Femoral growth after occlusion of the principal nutrient canal in day-old rabbits. J. Bone Joint Surg. Br. 39-B:563–571. The British Editorial Society of Bone & Joint Surgery.

Brookes, M. 1958. The vascular architecture of tubular bone in the rat. Anat. Rec. 132:25–47.

Brookes, M., and R. G. Harrison. 1957. The vascularization of the rabbit femur and tibiofibula. J. Anat. 91:61-72.2.

Cadney, M. D., L. Hiramatsu, Z. Thompson, M. Zhao, J. C. Kay, J. M. Singleton, R. L. de Albuquerque, M. P. Schmill, W. Saltzman, and T. Garland, Jr. 2021. Effects of early-life exposure to Western diet and voluntary exercise on adult activity levels, exercise physiology, and associated traits in selectively bred High Runner mice. Physiol. Behav. 234:113389.

Campos, F. F., G. L. Pellico, G. M. Alias, and R. Fernandez-Valencia. 1987. A study of the nutrient foramina in human long bones. Surg. Radiol. Anat. SRA 9:251–255.

Careau, V., M. E. Wolak, P. A. Carter, and T. Garland, Jr. 2013. Limits to behavioral evolution: the quantitative genetics of a complex trait under directional selection. Evolution 67:3102–3119.

Carroll, S. E. 1963. A study of the nutrient foramina of the humeral diaphysis. J. Bone Joint Surg. Br. 45-B:176–181.

Castro, A. A., F. A. Karakostis, L. E. Copes, H. E. McClendon, A. P. Trivedi, N. E. Schwartz, and T. Garland, Jr. 2022. Effects of selective breeding for voluntary exercise, chronic exercise, and their interaction on muscle attachment site morphology in house mice. J. Anat. 240:279–295.

Castro, A. A., H. Rabitoy, G. C. Claghorn, and T. Garland, Jr. 2021. Rapid and longer-term effects of selective breeding for voluntary exercise behavior on skeletal morphology in house mice. J. Anat. 238:720–742.

Chen, I. I., R. L. Prewitt, and R. F. Dowell. 1981. Microvascular rarefaction in spontaneously hypertensive rat cremaster muscle. Am. J. Physiol. 241:H306-310.

Copes, L. E., H. Schutz, E. M. Dlugosz, W. Acosta, M. A. Chappell, and T. Garland, Jr. 2015. Effects of voluntary exercise on spontaneous physical activity and food consumption in mice: Results from an artificial selection experiment. Physiol. Behav. 149:86–94.

Copes, L. E., H. Schutz, E. M. Dlugsoz, S. Judex, and T. Garland, Jr. 2018. Locomotor activity, growth hormones, and systemic robusticity: An investigation of cranial vault thickness in mouse lines bred for high endurance running. Am. J. Phys. Anthropol. 166:442–458.

Evans, S. F., J. B. Parent, C. E. Lasko, X. Zhen, U. R. Knothe, T. Lemaire, and M. L. Knothe Tate. 2013. Periosteum, bone's "smart" bounding membrane, exhibits direction-dependent permeability. J. Bone Miner. Res. Off. J. Am. Soc. Bone Miner. Res. 28:608–617.

Ferguson, V. L., R. A. Ayers, T. A. Bateman, and S. J. Simske. 2003. Bone development and age-related bone loss in male C57BL/6J mice. Bone 33:387–398.

Frost, H. M. 1987. Bone "mass" and the "mechanostat": a proposal. Anat. Rec. 219:1–9.

Frost, H. M. 1997. On our age-related bone loss: insights from a new paradigm. J. Bone Miner. Res. 12:1539–1546.

677 Gans, C. 1979. Momentarily excessive construction as the basis for protoadaptation. Evolution 33:227–
678 233.
679 Gardinier, J. D., N. Rostami, L. Juliano, and C. Zhang. 2018. Bone adaptation in response to treadmill
680 exercise in young and adult mice. Bone Rep. 8:29–37.
681 Garland, Jr., T., and P. W. Freeman. 2005. Selective breeding for high endurance running increases
682 hindlimb symmetry. Evol. Int. J. Org. Evol. 59:1851–1854.
683 Garland, Jr., T., S. A. Kelly, J. L. Malisch, E. M. Kolb, R. M. Hannon, B. K. Keeney, S. L. Van Cleave, and K. M.
684 Middleton. 2011. How to run far: multiple solutions and sex-specific responses to selective
685 breeding for high voluntary activity levels. Proc. R. Soc. B Biol. Sci. 278:574–581.
686 Garland, Jr., T., M. T. Morgan, J. G. Swallow, J. S. Rhodes, I. Girard, J. G. Belter, and P. A. Carter. 2002.
687 Evolution of a small-muscle polymorphism in lines of house mice selected for high activity levels.
688 Evol. Int. J. Org. Evol. 56:1267–1275.
689 Goligorsky, M. S. 2010. Microvascular rarefaction. Organogenesis 6:1–10.
690 Gómez-Cabello, A., I. Ara, A. González-Agüero, J. A. Casajús, and G. Vicente-Rodríguez. 2012. Effects of
691 training on bone mass in older adults. Sports Med. 42:301–325.
692 Greene, E. 1935. Anatomy of the rat. Trans. Am. Philos. Soc.
693 Gross, P. M., M. L. Marcus, and D. D. Heistad. 1981. Measurement of blood flow to bone and marrow in
694 experimental animals by means of the microsphere technique. J. Bone Joint Surg. Am. 63:1028–
695 1031.
696 Grüneboom, A., I. Hawwari, D. Weidner, S. Culemann, S. Müller, S. Henneberg, A. Brenzel, S. Merz, L.
697 Bornemann, K. Zec, M. Wuelling, L. Kling, M. Hasenberg, S. Voortmann, S. Lang, W. Baum, A. Ohs,
698 O. Kraff, H. H. Quick, M. Jäger, S. Landgraeber, M. Dudda, R. Danuser, J. V. Stein, M. Rohde, K.
699 Gelse, A. I. Garbe, A. Adamczyk, A. M. Westendorf, D. Hoffmann, S. Christiansen, D. R. Engel, A.
700 Vortkamp, G. Krönke, M. Herrmann, T. Kamradt, G. Schett, A. Hasenberg, and M. Gunzer. 2019. A

network of trans-cortical capillaries as mainstay for blood circulation in long bones. Nat. Metab. 1:236–250.

Gümüsburun, E., F. Yücel, Y. Ozkan, and Z. Akgün. 1994. A study of the nutrient foramina of lower limb long bones. Surg. Radiol. Anat. SRA 16:409–412.

Gupta, A. K., and M. N. Ambekar. 2016. Study of nutrient foramina in adult human femur bones. J. Nepalgunj Med. Coll. 14:44–49.

Henderson, R. G. 1978. The position of the nutrient foramen in the growing tibia and femur of the rat. J. Anat. 125:593–599.

Hillis, D. A., and T. Garland, Jr. 2023. Multiple solutions at the genomic level in response to selective breeding for high locomotor activity. Genetics 223:iyac165.

Hiramatsu, L., J. C. Kay, Z. Thompson, J. M. Singleton, G. C. Claghorn, R. L. Albuquerque, B. Ho, B. Ho, G. Sanchez, and T. Garland, Jr. 2017. Maternal exposure to Western diet affects adult body composition and voluntary wheel running in a genotype-specific manner in mice. Physiol. Behav. 179:235–245.

Houssaye, A., and J. Prévoteau. 2020. What about limb long bone nutrient canal(s)? – a 3D investigation in mammals. J. Anat. 236:510–521.

Hu, Q., T. J. Nelson, and R. S. Seymour. 2022. Morphology of the nutrient artery and its foramen in relation to femoral bone perfusion rates of laying and non-laying hens. J. Anat. 240:94–106.

Hu, Q., T. J. Nelson, E. P. Snelling, and R. S. Seymour. 2018. Femoral bone perfusion through the nutrient foramen during growth and locomotor development of western grey kangaroos (*Macropus fuliginosus*). J. Exp. Biol. 221:jeb168625.

Huiskes, R., R. Ruimerman, G. H. van Lenthe, and J. D. Janssen. 2000. Effects of mechanical forces on maintenance and adaptation of form in trabecular bone. Nature 405:704–706.

724 Jepsen, K. J., B. Hu, S. M. Tommasini, H.-W. Courtland, C. Price, M. Cordova, and J. H. Nadeau. 2009.
725 Phenotypic integration of skeletal traits during growth buffers genetic variants affecting the
726 slenderness of femora in inbred mouse strains. Mamm. Genome Off. J. Int. Mamm. Genome Soc.
727 20:21–33.
728 Jilka, R. L. 2013. The relevance of mouse models for investigating age-related bone loss in humans. J.
729 Gerontol. A. Biol. Sci. Med. Sci. 68:1209–1217.
730 Jones, H. H., J. D. Priest, W. C. Hayes, C. C. Tichenor, and D. A. Nagel. 1977. Humeral hypertrophy in
731 response to exercise. J. Bone Joint Surg. Am. 59:204–208.
732 Joo, Y.-I., T. Sone, M. Fukunaga, S.-G. Lim, and S. Onodera. 2003. Effects of endurance exercise on three-
733 dimensional trabecular bone microarchitecture in young growing rats. Bone 33:485–493.
734 Judex, S., R. Garman, M. Squire, B. Busa, L.-R. Donahue, and C. Rubin. 2004. Genetically linked site-
735 specificity of disuse osteoporosis. J. Bone Miner. Res. Off. J. Am. Soc. Bone Miner. Res. 19:607–
736 613.
737 Karlsson, M. K., and B. E. Rosengren. 2020. Exercise and peak bone mass. Curr. Osteoporos. Rep. 18:285–
738 290.
739 Katsimbri, P. 2017. The biology of normal bone remodeling. Eur. J. Cancer Care (Engl.) 26.
740 Kelly, S. A., T. A. Bell, S. R. Selitsky, R. J. Buus, K. Hua, G. M. Weinstock, T. Garland, Jr., F. Pardo-Manuel de
741 Villena, and D. Pomp. 2013. A novel intronic single nucleotide polymorphism in the *Myosin heavy*
742 *polypeptide 4* gene is responsible for the mini-muscle phenotype characterized by major
743 reduction in hind-limb muscle mass in mice. Genetics 195:1385–1395.
744 Kelly, S. A., P. P. Czech, J. T. Wight, K. M. Blank, and T. Garland, Jr. 2006. Experimental evolution and
745 phenotypic plasticity of hindlimb bones in high-activity house mice. J. Morphol. 267:360–374.

Kelly, S. A., F. R. Gomes, E. M. Kolb, J. L. Malisch, and T. Garland, Jr. 2017. Effects of activity, genetic selection and their interaction on muscle metabolic capacities and organ masses in mice. J. Exp. Biol. 220:1038–1047.

Knothe Tate, M. L., P. Niederer, and U. Knothe. 1998. In vivo tracer transport through the lacunocanalicular system of rat bone in an environment devoid of mechanical loading. Bone 22:107–117.

Kolb, E. M., S. A. Kelly, and T. Garland, Jr. 2013. Mice from lines selectively bred for high voluntary wheel running exhibit lower blood pressure during withdrawal from wheel access. Physiol. Behav. 112–113:49–55.

Laroche, M. 2002. Intraosseous circulation from physiology to disease. Joint Bone Spine 69:262–269.

Lewton, K. L., T. Ritzman, L. E. Copes, T. Garland, Jr., and T. D. Capellini. 2019. Exercise-induced loading increases ilium cortical area in a selectively bred mouse model. Am. J. Phys. Anthropol. 168:543–551.

Li, G., J. T. Bronk, K.-N. An, and P. J. Kelly. 1987. Permeability of cortical bone of canine tibiae. Microvasc. Res. 34:302–310.

Liang, J., Y. Li, L. Chen, W. Xia, G. Wu, X. Tong, C. Su, J. He, X. Lin, and J. Tao. 2019. Systemic microvascular rarefaction is correlated with dysfunction of late endothelial progenitor cells in mild hypertension: a substudy of EXCAVATION-CHN1. J. Transl. Med. 17:368.

Meek, T. H., B. P. Lonquich, R. M. Hannon, and T. Garland, Jr. 2009. Endurance capacity of mice selectively bred for high voluntary wheel running. J. Exp. Biol. 212:2908–2917.

Middleton, K. M., B. D. Goldstein, P. R. Guduru, J. F. Waters, S. A. Kelly, S. M. Swartz, and T. Garland, Jr. 2010. Variation in within-bone stiffness measured by nanoindentation in mice bred for high levels of voluntary wheel running. J. Anat. 216:121–131.

769 Middleton, K. M., C. E. Shubin, D. C. Moore, P. A. Carter, T. Garland, Jr., and S. M. Swartz. 2008. The
770 relative importance of genetics and phenotypic plasticity in dictating bone morphology and
771 mechanics in aged mice: evidence from an artificial selection experiment. Zool. Jena Ger.
772 111:135–147.
773 Mori, T., N. Okimoto, A. Sakai, Y. Okazaki, N. Nakura, T. Notomi, and T. Nakamura. 2003. Climbing exercise
774 increases bone mass and trabecular bone turnover through transient regulation of marrow
775 osteogenic and osteoclastogenic potentials in mice. J. Bone Miner. Res. 18:2002–2009.
776 Newhall, K. M., K. J. Rodnick, M. C. van der Meulen, D. R. Carter, and R. Marcus. 1991. Effects of voluntary
777 exercise on bone mineral content in rats. J. Bone Miner. Res. Off. J. Am. Soc. Bone Miner. Res.
778 6:289–296.
779 Payton, C. G. 1934. The position of the nutrient foramen and direction of the nutrient canal in the long
780 bones of the madder-fed pig. J. Anat. 68:500–510.
781 Prewitt, R. L., H. Hashimoto, and D. L. Stacy. 1989. Structural and functional rarefaction of microvessels in
782 hypertension. Pp. 71–79 *in* Blood Vessel Changes in Hypertension Structure and Function. CRC
783 Press.
784 Prisby, R. D. 2020. Bone marrow microvasculature. Compr. Physiol. 10:1009–1046.
785 Prisby, R. D., B. J. Behnke, M. R. Allen, and M. D. Delp. 2015. Effects of skeletal unloading on the
786 vasomotor properties of the rat femur principal nutrient artery. J. Appl. Physiol. 118:980–988.
787 Qin, Y. X., T. Kaplan, A. Saldanha, and C. Rubin. 2003. Fluid pressure gradients, arising from oscillations in
788 intramedullary pressure, is correlated with the formation of bone and inhibition of intracortical
789 porosity. J. Biomech. 36:1427–1437.
790 Rhinelander, F. W. 1972. Circulation in bone. Pp. 1–77 *in* The Biochemistry and Physiology of Bone.
791 Academic Press, New York.

792 Rhodes, J. S., S. C. Gammie, and T. Garland, Jr. 2005. Neurobiology of mice selected for high voluntary
793 wheel-running activity. Integr. Comp. Biol. 45:438–455.
794 Rodrigues, J., Y.-F. Wang, A. Singh, M. Hendriks, G. Dharmalingam, M. Cohen-Solal, A. P. Kusumbe, and S.
795 K. Ramasamy. 2022. Estrogen enforces the integrity of blood vessels in the bone during pregnancy
796 and menopause. Nat. Cardiovasc. Res. 1:918–932. Nature Publishing Group.
797 Rogers, W. M., and H. Gladstone. 1950. Vascular foramina and arterial supply of the distal end of the
798 femur. J. Bone Joint Surg. Am. 32 A:867–874.
799 Rosei, E. A., and D. Rizzoni. 2007. The effects of hypertension on the structure of human resistance
800 vessels. Pp. 579–589 *in* G. Y. H. Lip and J. E. Hall, eds. Comprehensive Hypertension. Mosby,
801 Philadelphia.
802 Rubin, C. T., and L. E. Lanyon. 1984. Regulation of bone formation by applied dynamic loads. J. Bone Joint
803 Surg. Am. 66:397–402.
804 Rumney, R. M. H., S. A. Lanham, J. M. Kanczler, A. P. Kao, L. Thiagarajan, J. E. Dixon, G. Tozzi, and R. O. C.
805 Oreffo. 2019. In vivo delivery of VEGF RNA and protein to increase osteogenesis and intraosseous
806 angiogenesis. Sci. Rep. 9:17745. Nature Publishing Group.
807 Schneider, C. A., W. S. Rasband, and K. W. Eliceiri. 2012. NIH Image to ImageJ: 25 years of image analysis.
808 Nat. Methods 9:671–675.
809 Schutz, H., H. A. Jamniczky, B. Hallgrímsson, and T. Garland, Jr. 2014. Shape-shift: semicircular canal
810 morphology responds to selective breeding for increased locomotor activity. Evol. Int. J. Org. Evol.
811 68:3184–3198.
812 Schwartz, N. E., M. P. McNamara, J. M. Orozco, J. O. Rashid, A. P. Thai, and T. Garland Jr. 2023. Selective
813 breeding for high voluntary exercise in mice increases maximal ($\dot{V}O_{2,max}$) but not basal metabolic
814 rate. J. Exp. Biol. 226:jeb245256.

Schwartz, N. E., B. A. Patel, T. Garland, Jr., and A. M. Horner. 2018. Effects of selective breeding for high voluntary wheel-running behavior on femoral nutrient canal size and abundance in house mice. J. Anat. 233:193–203.

Seref-Ferlengez, Z., O. D. Kennedy, and M. B. Schaffler. 2015. Bone microdamage, remodeling and bone fragility: how much damage is too much damage? BoneKEy Rep. 4:644.

Seymour, R. S., S. L. Smith, C. R. White, D. M. Henderson, and D. Schwarz-Wings. 2012. Blood flow to long bones indicates activity metabolism in mammals, reptiles and dinosaurs. Proc. R. Soc. B Biol. Sci. 279:451–456.

Sim, F. H., and P. J. Kelly. 1970. Relationship of bone remodeling, oxygen consumption, and blood flow in bone. J. Bone Joint Surg. Am. 52:1377–1389.

Singh, I., H. Sandhu, and M. Herskovits. 1991. Bone vascularity. Pp. 141–157 *in* B. Hall, ed. Bone Matrix and Bone Specific Products. CRC Press, Boca Raton.

Singleton, J. M., and T. Garland, Jr. 2019. Influence of corticosterone on growth, home-cage activity, wheel running, and aerobic capacity in house mice selectively bred for high voluntary wheel-running behavior. Physiol. Behav. 198:27–41.

Stabley, J. N., N. C. Moningka, B. J. Behnke, and M. D. Delp. 2014. Exercise training augments regional bone and marrow blood flow during exercise. Med. Sci. Sports Exerc. 46:2107–2112.

Swallow, J. G., P. A. Carter, and T. Garland, Jr. 1998a. Artificial selection for increased wheel-running behavior in house mice. Behav. Genet. 28:227–237.

Swallow, J. G., and T. Garland, Jr. 2005. Selection experiments as a tool in evolutionary and comparative physiology: insights into complex traits--an introduction to the symposium. Integr. Comp. Biol. 45:387–390.

837 Swallow, J. G., T. Garland, Jr., P. A. Carter, W.-Z. Zhan, and G. C. Sieck. 1998b. Effects of voluntary activity
838 and genetic selection on aerobic capacity in house mice (*Mus domesticus*). J. Appl. Physiol. 84:69–
839 76.
840 Swallow, J. G., P. Koteja, P. A. Carter, and T. Garland, Jr. 2001. Food consumption and body composition in
841 mice selected for high wheel-running activity. J. Comp. Physiol. [B] 171:651–659.
842 Talmadge, R. J., W. Acosta, and T. Garland, Jr. 2014. Myosin heavy chain isoform expression in adult and
843 juvenile Mini-Muscle mice bred for high-voluntary wheel running. Mech. Dev. 134:16–30.
844 Tommasini, S. M., S. L. Wearne, P. R. Hof, and K. J. Jepsen. 2008. Percolation theory relates
845 corticocancellous architecture to mechanical function in vertebrae of inbred mouse strains. Bone
846 42:743–750.
847 Trueta, J. 1963. The role of the vessels in osteogenesis. J. Bone Joint Surg. Br. 45-B:402–418. The British
848 Editorial Society of Bone & Joint Surgery.
849 Wallace, I. J., and T. Garland, Jr. 2016. Mobility as an emergent property of biological organization:
850 Insights from experimental evolution: Mobility and biological organization. Evol. Anthropol. Issues
851 News Rev. 25:98–104.
852 Wallace, I. J., S. M. Tommasini, S. Judex, T. Garland, Jr., and B. Demes. 2012. Genetic variations and
853 physical activity as determinants of limb bone morphology: An experimental approach using a
854 mouse model. Am. J. Phys. Anthropol. 148:24–35.
855 Yang, L., P. Zhang, S. Liu, P. R. Samala, M. Su, and H. Yokota. 2007. Measurement of strain distributions in
856 mouse femora with 3d-digital speckle pattern interferometry. Opt. Lasers Eng. 45:843–851.
857 Young, N. M., B. Hallgrímsson, and T. Garland, Jr. 2009. Epigenetic effects on integration of limb lengths in
858 a mouse model: selective breeding for high voluntary locomotor activity. Evol. Biol. 36:88.
859 Yu, K., D. P. Sellman, A. Bahraini, M. L. Hagan, A. Elsherbini, K. T. Vanpelt, P. L. Marshall, M. W. Hamrick, A.
860 McNeil, P. L. McNeil, and M. E. McGee-Lawrence. 2018. Mechanical loading disrupts osteocyte

plasma membranes which initiates mechanosensation events in bone. J. Orthop. Res. Off. Publ. Orthop. Res. Soc. 36:653–662.

Yuan, Y., X. Chen, L. Zhang, J. Wu, J. Guo, D. Zou, B. Chen, Z. Sun, C. Shen, and J. Zou. 2016. The roles of exercise in bone remodeling and in prevention and treatment of osteoporosis. Prog. Biophys. Mol. Biol. 122:122–130.

Supplementary Material

Illustrated, in-depth instructions for measuring nutrient canals in AMIRA:

Nutrient_Canal_Methods_Presentation_6.pdf

Full results from multiple statistical models (Supplemental Table S1):

NC_Tables_SAS_26_Hidden_UPLOAD.xlsx

TABLE 1 Results from mixed models for body mass and femur length (SAS PROCEDURE MIXED).

				Linetype effects			Activity			Linetype x Activity			Mini-muscle effects			Body length				Body mass			
Variable	*n*	*transform or modification*	Skew	df	*F*	*P*	df	*F*	*P*	df	*F*	*P*	df	*F*	*P*	df	*F*	*P*	Slope	df	*F*	*P*	Slope
Body Mass	94	N/A	0.26	1,6	4.64	0.0748	1,6	3.53	0.1092	1,6	0.62	0.4612	1,77	0.30	0.5836								
Body Mass	91	N/A	0.15	1,6	4.16	0.0874	1,6	1.07	0.3406	1,6	0.02	0.8842	1,73	0.58	0.4474	1,73	37.60	**<.0001**	+				
Body Length	91	N/A	0.21	1,6	3.78	0.0999	1,6	1.40	0.2810	1,6	2.14	0.1940	1,74	0.69	0.4095								
Femur Length	89	N/A	-0.18	1,6	0.05	0.8245	1,6	0.08	0.7844	1,6	0.11	0.7520	1,71	0.12	0.7318	1,71	21.46	**<.0001**	+				
Femur Length	92	N/A	-0.57	1,6	0.07	0.7987	1,6	0.06	0.8140	1,6	0.00	0.9460	1,74	0.21	0.6482					1,74	56.85	**<.0001**	+

Significance levels (P values; **bold** indicates $P < 0.05$, unadjusted for multiple comparisons) from two-way nested analysis of covariance models implemented in SAS PROC MIXED.

TABLE 2 Results from mixed models for nutrient canal characteristics (SAS PROCEDURE MIXED or GLIMMIX).

				Linetype effects			Activity			Linetype x Activity			Mini-muscle effects			Mass			
Variable	*n*	*transform or modification*	Skew	df	*F*	*P*	df	*F*	*P*	df	*F*	*P*	df	*F*	*P*	df	*F*	*P*	Slope
Total area (mm^2)	94	N/A	0.33	1,6	0.01	0.9236	1,6	3.40	0.1148	1,6	1.46	0.2730	1,76	0.12	0.7248	1,76	1.65	0.2026	
Proximal area (mm2)	93	Outlier	0.20	1,6	0.00	0.9933	1,6	2.37	0.1743	1,6	0.42	0.5405	1,75	1.26	0.2652	1,75	1.54	0.2186	
Distal area (mm^2)	94	N/A	0.24	1,6	0.02	0.8919	1,6	0.64	0.4539	1,6	2.27	0.1827	1,76	1.06	0.3069	1,76	9.27	**0.0032**	**+**
Percent distal CSA	94	N/A	0.04	1,6	0.21	0.6657	1,6	0.01	0.9351	1,6	0.65	0.4510	1,76	0.41	0.5252	1,76	4.65	**0.0342**	**+**
Total number	94	Log10	-0.06	1,6	0.72	0.4272	1,6	1.55	0.2593	1,6	10.56	**0.0175**	1,76	1.02	0.3146	1,76	0.17	0.6773	
Proximal number	94	N/A	0.33	1,6	2.71	0.1511	1,6	0.55	0.4877	1,6	2.91	0.1387	1,76	0.97	0.3268	1,76	5.76	**0.0188**	**-**
Distal Number	94	Log10	0.16	1,6	0.41	0.5471	1,6	0.58	0.4769	1,6	3.92	0.0949	1,76	0.94	0.3351	1,76	8.14	**0.0056**	**+**
Percent distal number	94	N/A	0.35	1,6	2.77	0.1469	1,6	0.65	0.4495	1,6	0.64	0.4553	1,76	2.50	0.1180	1,76	10.64	**0.0017**	**+**
Average proximal location	93	Log10	0.22	1,6	0.01	0.9217	1,6	1.45	0.2737	1,6	0.40	0.5497	1,75	0.84	0.3611	1,75	0.96	0.3294	
Average distal location	88	Power 2	-0.32	1,6	0.60	0.4669	1,6	0.18	0.6880	1,6	0.02	0.8982	1,70	0.72	0.3981	1,70	4.48	**0.0379**	**-**
Average CSA per canal	94	Log10	-0.35	1,6	0.57	0.4787	1,6	0.21	0.6619	1,6	1.76	0.2324	1,76	0.16	0.6930	1,76	0.14	0.7051	
Proximal avg CSA per canal	94	Rank	-0.04	1,6	1.18	0.3196	1,6	0.87	0.3859	1,6	0.89	0.3828	1,76	0.07	0.7990	1,76	0.06	0.8079	
Distal avg CSA per canal	94	Rank	0.05	1,6	0.72	0.4300	1,6	0.06	0.8186	1,6	0.09	0.7792	1,76	0.28	0.5972	1,76	0.01	0.9407	
Percent Curved Canal Number	94	Power 0.7	-0.23	1,6	1.25	0.3067	1,6	3.07	0.1303	1,6	0.29	0.6091	1,76	0.46	0.4997	1,76	0.00	0.9623	

Significance levels (P values; **bold** indicates $P < 0.05$, unadjusted for multiple comparisons) from two-way nested analysis of covariance models implemented in SAS PROC MIXED.

TABLE 3 Results from mixed models for nutrient canal bifurcations (SAS PROCEDURE GLIMMIX).

				Linetype effects			Activity			Linetype x Activity			Mini-muscle effects			Mass		
Variable	*n*	*transform or modification*		df	*F*	*P*	df	*F*	*P*	df	*F*	*P*	df	*F*	*P*	df	*F*	*P*
Bifurcated number (Line nested)	94	N/A		1,6	3.59	0.1070	1,6	1.46	0.2717	1,6	1.88	0.2192	1,76	0.70	0.4049	1,76	0.14	0.7123
Bifurcated number (Line nested)	94	N/A		1,6	5.18	0.0631	1,6	1.54	0.2606	1,6	1.81	0.2266	1,77	0.64	0.4252			
Bifurcated number (Line not nested)	94	N/A		1,88	3.59	0.0614	1,88	1.46	0.2294	1,88	1.88	0.1736	1,88	0.70	0.4046	1,88	0.14	0.7122
Bifurcated number (Line not nested)	94	N/A		1,89	5.18	**0.0252**	1,89	1.54	0.2175	1,89	1.81	0.1814	1,89	0.64	0.4249			

Significance levels (P values; bold indicates P < 0.05, unadjusted for multiple comparisons) from mixed models in SAS PROC GLIMMIX analyzing the presence/absence of any bifurcated nutrient canals, with and without body mass as a covariate. If line is not considered as a nested random effect within linetype, then statistical significance is attained for the linetype effect.

TABLE 4 Summary of results for bone traits analyzed for this set of mice.

Reference	Linetype (HR vs. C lines)	Activity	Linetype-by-Activity Interaction	Mini-muscle	Body Mass
Copes et al. 2018	0/12 (0%)	0/12 (0%)	0/12 (0%)	2/12 (17%)	10/12 (83%)
Lewton et al. 2019	0/6 (0%)	2/6 (33%)	0/6 (0%)	5/6 (83%)	6/6 (100%)
Castro et al. 2022	0/4 (0%)	1/4 (25%)	0/4 (0%)	1/4 (25%)	3/4 (75%)
This Study of Canals	0/14 (0%)	0/14 (0%)	1/14 (7%)	0/14 (0%)	6/14 (43%)
Total	0/36 (0%)	3/36 (8%)	1/36 (3%)	8/36 (22%)	26/36 (72%)

Summary of statistical results for four studies that have measured bone traits in the same set of female mice from generation 57 of the High Runner selection experiment. Overall, the present study found fewer statistically significant effects than the other three studies. Cell entries are the number of P values < 0.05 divided by the total number of traits. Body mass was used as a covariate in all analyses compared here.

FIGURE 1 Zone within which femoral nutrient canals were measured.

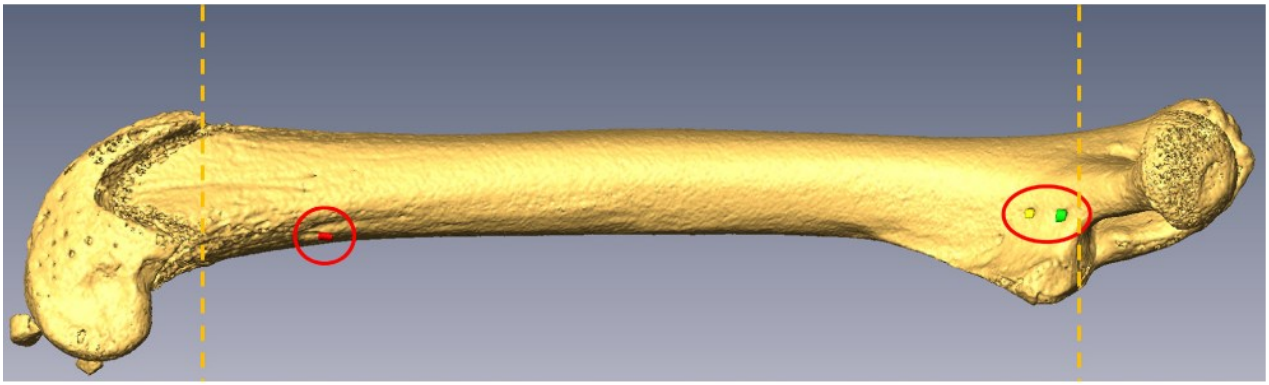

3D model of mouse femur, medial view, with distal end on the left, and proximal end on the right. Nutrient canals are circled in red. Following Schwartz et al. (2018), measurements were restricted to the region above the patellar groove and below the base of the femoral neck (as indicated by the yellow dashed lines) to prevent inclusion of metaphyseal and periosteal vessels which frequently penetrate bone outside this defined area.

FIGURE 2 Example of a femoral nutrient canal seen across serial CT scan slices.

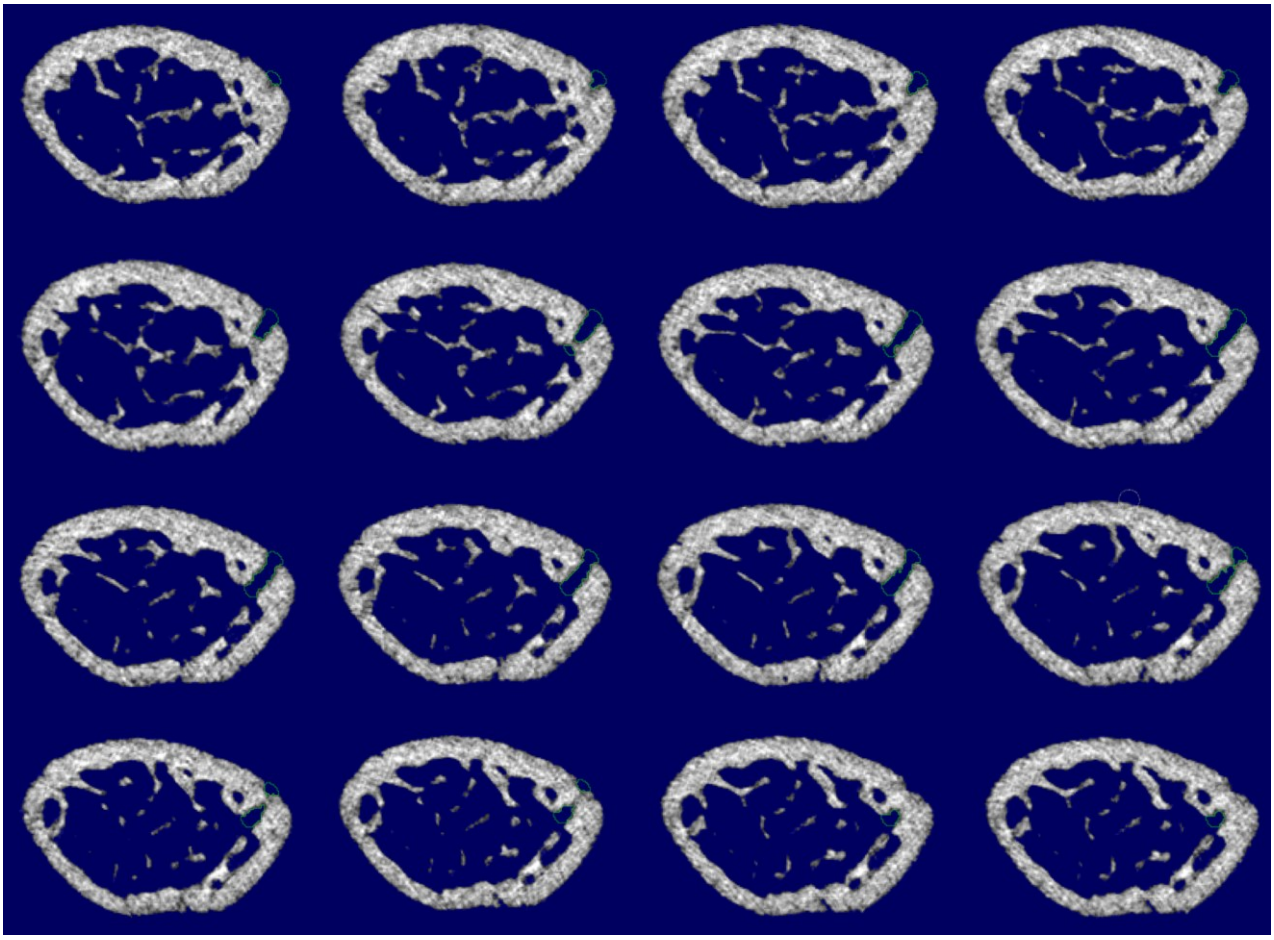

Sequential transverse slices of a mouse femur showing the nutrient canal (outlined in green).

FIGURE 3 Re-oriented nutrient canals of various shapes with transverse slices.

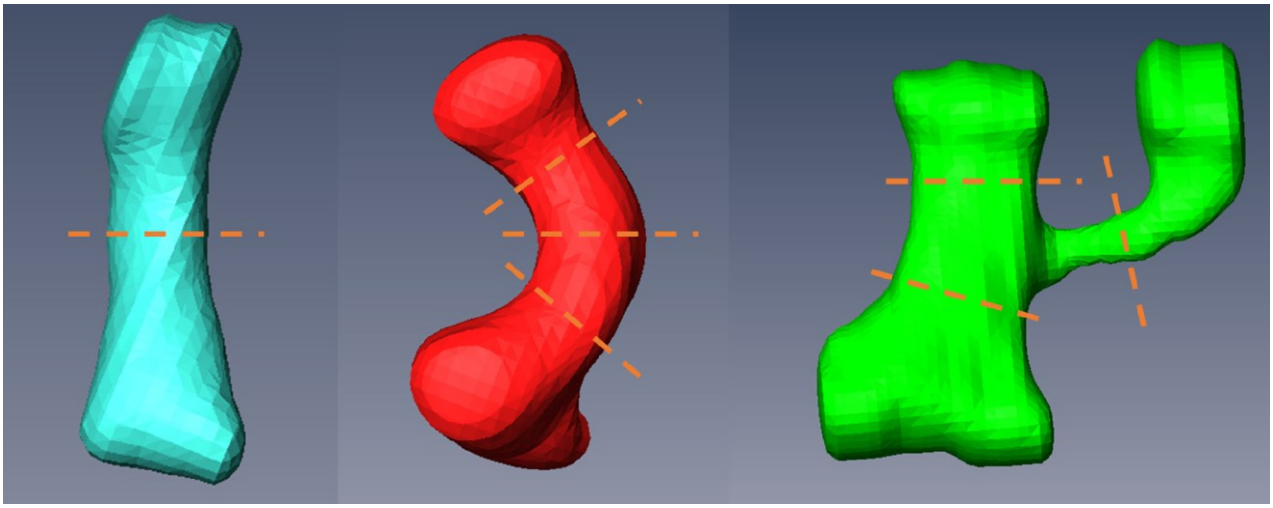

3D models of femoral nutrient canals, re-oriented to properly measure the transverse slices for cross-sectional area. Many different nutrient canal shapes were encountered, including, straight, curved, and branched. Mouse identification numbers are (left to right) 60204 (Line HR7), 60275 (Line C4), 60447 (Line C2).

FIGURE 4 Nutrient canal characteristics in relation to body mass.

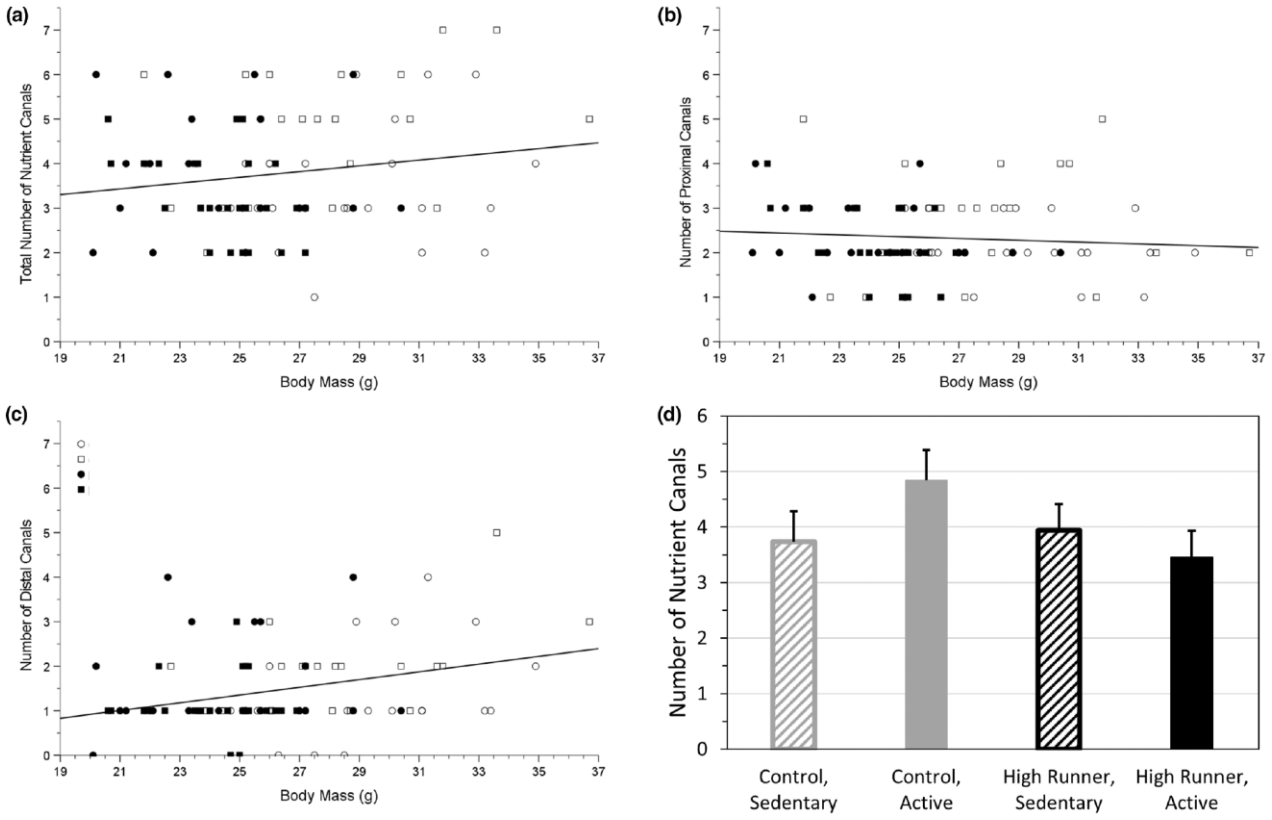

Relation between (A) total canal number, (B) proximal canal number, and (C) distal canal number and body mass for mice from four experimental groups (see text). Solid lines are simple least-squares linear regressions. Body mass was a negative predictor of proximal number (P = 0.0188) but a positive predictor of distal number (P = 0.0056), resulting in no significant relation with total canal number (P = 0.6773). With body mass as a covariate, total canal number was affected by an interaction between linetype and wheel access (P = 0.0175): voluntary exercise increased numbers in C mice, but decreased numbers in HR mice (Table 2 and panel D, which shows least squares means and standard errors from SAS procedure Mixed). The interaction also affected proximal and distal numbers of canals in the same manner, but statistical significance was not attained (P = 0.1378 and 0.0949, respectively).